

# Measurement of spin-flip probabilities for ultracold neutrons interacting with nickel phosphorus coated surfaces

Z. Tang<sup>a</sup>, E. R. Adamek<sup>b</sup>, A. Brandt<sup>c</sup>, N. B. Callahan<sup>b</sup>, S. M. Clayton<sup>a</sup>, S. A. Currie<sup>a</sup>, T. M. Ito<sup>a,\*</sup>, M. Makela<sup>a</sup>, Y. Masuda<sup>d</sup>, C. L. Morris<sup>a</sup>, R. Pattie Jr.<sup>a</sup>, J. C. Ramsey<sup>a</sup>, D. J. Salvat<sup>a,b</sup>, A. Saunders<sup>a</sup>, A. R. Young<sup>c</sup>

<sup>a</sup>*Los Alamos National Laboratory, Los Alamos, New Mexico 87545, USA*

<sup>b</sup>*Indiana University, Bloomington, Indiana 47405, USA*

<sup>c</sup>*North Carolina State University, Raleigh, North Carolina, 27695, USA*

<sup>d</sup>*High Energy Accelerator Research Organization, Tsukuba, Ibaraki 305-0801, Japan*

---

## Abstract

We report a measurement of the spin-flip probabilities for ultracold neutrons interacting with surfaces coated with nickel phosphorus. For 50  $\mu\text{m}$  thick nickel phosphorus coated on stainless steel, the spin-flip probability per bounce was found to be  $\beta_{\text{NiP on SS}} = (3.3^{+1.8}_{-5.6}) \times 10^{-6}$ . For 50  $\mu\text{m}$  thick nickel phosphorus coated on aluminum, the spin-flip probability per bounce was found to be  $\beta_{\text{NiP on Al}} = (3.6^{+2.1}_{-5.9}) \times 10^{-6}$ . For the copper guide used as reference, the spin flip probability per bounce was found to be  $\beta_{\text{Cu}} = (6.7^{+5.0}_{-2.5}) \times 10^{-6}$ . Nickel phosphorus coated stainless steel or aluminum provides a solution when UCN guides that have a high Fermi potential and are low-cost, mechanically robust, and non-depolarizing are needed.

*Keywords:*

---

## 1. Introduction

Ultra-cold neutrons (UCNs) are defined operationally to be those neutrons whose kinetic energies are sufficiently low so that they can be confined in a material bottle, corresponding to kinetic energies below about 340 neV. UCNs are playing increasingly important roles in providing answers to some of the most profound questions in physics. (For recent reviews, see *e.g.* Refs. [1, 2].)

Experiments using UCN are being performed at UCN facilities around the world, including Institut Laue-Langevin (ILL) [3], Los Alamos National Laboratory (LANL) [4], Research Center for Nuclear Physics (RCNP) at Osaka University [5], Paul Scher-

rer Institut (PSI) [6], and University of Mainz [7]. One important component for experiments at such facilities is the UCN transport guides. These UCN guides are used to transport UCNs from a UCN source to experiments and also from one part of an experiment to another. For applications that require spin polarized UCNs, it is important that UCNs retain their polarization as they are transported (see *e.g.* Ref. [12]).

In other applications in which polarized UCNs are stored for extended periods of time, such as neutron electric dipole moment experiments (see *e.g.* Ref. [13]) and the UCNA experiment (see *e.g.* Ref. [14]), it is also important that UCNs remain highly polarized while they are stored in a UCN bottle. In some cases, the depolarization of UCNs due to wall collisions is one of the dominant sources of systematic uncertainties in the final result of an ex-

---

\*Corresponding author

Email address: ito@lanl.gov (T. M. Ito)

periment [15].

Because of its importance for these applications, the study of the spin-flip probabilities and the possible mechanisms for spin flip is an active area of research [8, 9, 10, 11]. The spin-flip probability per bounce has been measured for various materials. References [8, 10] report results on beryllium, quartz, beryllium oxide, glass, graphite, brass, copper, and Teflon, whereas Ref. [11] discusses results on diamond-like carbon (DLC) coated on aluminum foil and on polyethyleneterephthalate (PET) foil. In addition measurements of the spin-flip probability per bounce have been performed for DLC coated quartz [16], stainless steel, electropolished copper, and DLC coated copper [17]. (The results from Ref. [17] are available in Ref. [18].) The reported values for the spin-flip probability per bounce are on the order of  $10^{-6} - 10^{-5}$  for all materials with an exception of stainless steel, for which the reported preliminary value for the spin-flip probability per bounce was on the order of  $10^{-3}$  [17], two to three orders of magnitude larger than for other materials.

The spin-flipping elastic or quasielastic incoherent scattering from protons of the surface hydrogen contamination has been considered to be a possible mechanism for UCN spin flip upon interaction with a surface [8, 9, 10, 11]. So far, however, data and model calculations have not been in agreement.

Another possible mechanism is Majorana spin flip [19] due to magnetic field inhomogeneity near material surfaces, due to ferromagnetic impurities or magnetization of the material itself. In addition, the sudden change in direction that occurs when a UCN reflects from a surface can cause a spin flip in the presence of moderate gradients [9]. Gamblin and Carver [20] discuss such an effect for  $^3\text{He}$  atoms. The large spin-flip probability observed for stainless steel in a large holding field [17] is likely to be due to magnetic field inhomogeneity near material surfaces magnetization of the material itself.

Recently, based on the suggestion from Ref. [21], we have identified nickel phosphorus (NiP) coating to be a promising UCN coating material with a small loss per bounce and a high Fermi potential [22]. NiP with a phosphorus content of 12% by weight and a density of  $7.6 \text{ g/cm}^3$  is calculated to give a Fermi po-

tential of 210 neV, to be compared to 188 neV for stainless steel and 168 neV for copper. NiP coating is extremely robust and is widely used in industrial applications. It is highly attractive from a practical point of view because the coating can be done commercially in a rather straightforward chemical process and there are numerous vendors that can provide such a service rather inexpensively. Note that it is important that the coating process not use neutron absorbing materials such as cadmium. When made with high phosphorus content, it is known to be non-magnetic. Therefore, it is of great interest to study its UCN spin depolarization property. In addition, it is also of interest to study how the depolarization depends on the material used for the substrate.

In this paper, we report a measurement of the spin-flip probabilities for UCNs interacting with NiP coated surface. We used aluminum and stainless steel as the substrate. The results obtained with NiP coated surfaces were compared to those obtained with copper guides. This measurement was done as part of development work for a new neutron electric dipole moment experiment at the LANL UCN facility [23] and the associated UCN source upgrade [24].

This paper is organized as follows. In Sec. 2, the experimental apparatus and method are described. Section 3 describes the analysis of the data. In Sec. 4, we discuss the implication of the results on future experiments using UCN. Section 5 provides a short summary of the content of this paper.

## 2. Experiment

### 2.1. Apparatus and method

The measurement was performed at the LANL UCN facility [4]. Spallation neutrons produced by a pulsed 800 MeV proton beam striking on a tungsten target were moderated by beryllium and graphite moderators at the ambient temperature and were further cooled by a cold moderator that consisted of cooled polyethylene beads. The cold neutrons were converted to UCNs by the solid deuterium ( $\text{SD}_2$ ) converter. UCNs were then directed upward 1 m along the vertical UCN guide coated with  $^{58}\text{Ni}$  and then 6 m along the horizontal guide made of stainless steel out

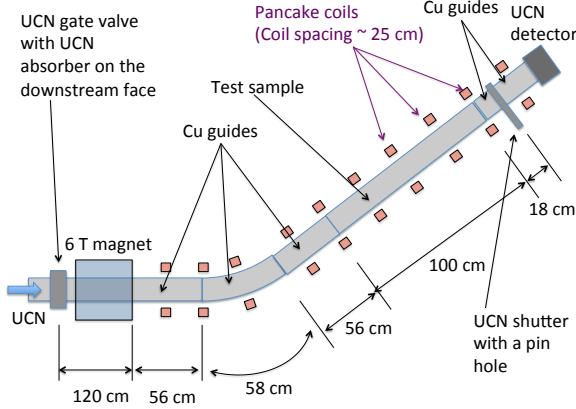


Figure 1: Schematic of the experimental setup

of the biological shield. At the bottom of the vertical UCN guide was a butterfly valve that remained closed when there was no proton beam pulse striking on the spallation target in order to keep the UCNs from returning to the SD<sub>2</sub> to be absorbed.

A schematic of the experimental setup for the depolarization measurement is shown in Fig. 1. When the UCN gate valve was opened, UCNs transported from the UCN source entered the apparatus. UCNs in one spin state, the so-called “high-field seekers” for which  $\boldsymbol{\mu} \cdot \mathbf{B} < 0$  where  $\boldsymbol{\mu}$  is the magnetic dipole moment of the neutron, were able to move past the 6 T magnetic field provided by a superconducting solenoidal magnet. UCNs in the other spin state, the so-called “low-field seekers” were reflected back by the potential barrier due to  $\boldsymbol{\mu} \cdot \mathbf{B} > 0$ . (Note for  $|\mathbf{B}| = 6$  T,  $|\boldsymbol{\mu} \cdot \mathbf{B}| = 360$  neV, larger than the kinetic energy of the neutrons from the LANL UCN source.)

On the other side of the high-field region was a 76.2 mm OD UCN guide system that consisted of a set of copper guide sections, a NiP coated guide section, and a section of a copper guide with a UCN shutter, a short section of a copper guide, followed by a UCN detector. The guides were placed in a  $\sim 20$  gauss magnetic field provided by a set of coils in order to retain the polarization of the UCNs. The UCN shutter had a pinhole 5 mm in diameter.

The high-field seekers were able to move freely through the high magnetic field region, colliding with

the inner walls of the guide system. The number of collisions per second for the high-field seekers in the guide system downstream of the 6 T field region is given by

$$R_{hfs} = \frac{1}{4} A_{tot} \langle v_{hfs} \rangle n_{hfs}, \quad (1)$$

where  $A_{tot}$  is the total inner surface of the system that the high field seekers interacted with in the guide system downstream of the 6 T field region,  $\langle v_{hfs} \rangle$  is the average velocity of the high-field seekers, and  $n_{hfs}$  is the density of the high-field seekers. The rate of collisions for the high field seekers was monitored during this time by detecting neutrons that leaked through a pinhole on the shutter in the downstream end of the set up. If UCNs are detected at a rate of  $R_h$  and the area of the pinhole is  $A_h$ ,  $R_{hfs}$  can be inferred to be

$$R_{hfs} = \frac{A_{tot}}{A_h} R_h, \quad (2)$$

assuming that the distribution of UCNs inside the system is uniform and isotropic.

While the high-field seekers collided with the inner wall of the system at the rate of  $R_{hfs}$ , spin-flipped neutrons were produced at a rate of

$$R_{dep} = R_{hfs} \beta = \frac{A_{tot}}{A_h} R_h \beta, \quad (3)$$

where  $\beta$  is the probability of spin flip per bounce. While, in principle,  $\beta$  can depend on the neutron velocity as well as the angle of incidence, and such dependences can give important information on the possible mechanism of UCN depolarization upon wall collision, we assumed  $\beta$  to be independent of the velocity and angle of incidence in our analysis. Note that Ref. [11] observed no indication of energy dependence within the accuracy of their measurement for the depolarization per bounce on DLC.

The spin-flipped neutrons were no longer able to pass through the 6 T field region freely and hence became “trapped” in the guide assembly downstream of the 6 T field region. If  $R_{hfs}$  was constant, then the number of the spin-flipped low-field seekers built up as  $[1 - \exp(-t/\tau_{dep})]$ , where  $\tau_{dep}$  is the lifetime of the spin-flipped neutrons.

The UCN gate valve was then closed, after which time the high-field seekers were quickly absorbed by the UCN absorber attached to the downstream side of the gate valve. On the other hand, the spin-flipped low-field seekers remained trapped in the volume between the 6 T field and the UCN shutter.

Opening the shutter allowed the trapped spin-flipped UCN to be detected by the UCN detector.

If the UCN gate valve initially remained open for loading time  $T_L$ , followed by cleaning time  $T_C$  during which time both the UCN gate valve and the UCN shutter remained closed and at the end of which the UCN shutter was opened, the number of the detected spin-flipped neutrons is given by

$$N_{dep} = \beta \frac{A_{tot}}{A_h} \int_0^{T_L+T_C} \int_0^{v_c} P(v, t) R_h(t) e^{-\frac{T_L+T_C-t}{\tau_{dep}(v)}} dv dt, \quad (4)$$

where  $P(v, t)$  is the velocity distribution of UCNs at the time of spin flip,  $v_c$  is the cutoff energy, and  $\tau_{dep}(v)$  is the lifetime of the depolarized neutrons, which in general is a function of the UCN velocity  $v$ . Since both the high-field seekers and the spin-flipped low-field seekers are detected by the same UCN detector, the possible finite detection efficiency drops off from the expression. Measuring  $N_{dep}$  and  $R_h(t)$ , with sufficient knowledge of  $P(v, t)$  and  $\tau_{dep}(v)$ , would determine  $\beta$ .

The currents for the coils providing the holding field were adjusted so that the field was higher than 20 gauss and the gradient was smaller than 100 gauss/cm to ensure that the probability of Majorana spin flip due to UCN passing an inhomogeneous field region or due to wall collision in an inhomogeneous field was less than  $10^{-6}$  per pass/bounce [19].

As seen in Fig. 1 and Table 1, a large portion of the guide system downstream of the 6 T field was made of copper. Copper was chosen because its spin-flip probability was determined to be low by previous measurements. The fraction of the UCN interacting surface due to the test sample was only  $\sim 35\%$ , diluting the sensitivity to the spin flip due to the test sample. This was due to the geometrical constraints in the experimental area.

## 2.2. Sample preparation

Two NiP coated samples were prepared, one on a 316L stainless steel tube and the other on an aluminum tube. Both tubes had an ID of 2.87" (7.29 cm). The 316L stainless steel tube was cut from welded tubing that has been polished and electropolished to 10Ra, purchased from Valex (specification 401) [25]. The aluminum tube was cut from unpolished 6061-T6511 aluminum tubing.

The coating was done using high-phosphorus content electroless nickel phosphorus plating. The phosphorus content was 10-13%. The thickness of the coating was 50  $\mu\text{m}$  for both samples. Post-baking at 375°C for 20 hours was performed for both samples. The coated surface was then cleaned by the following cleaning procedure:

1. The samples were submerged in alconox solution (1% by weight) at 60° for 10 hours.
2. The samples were then rinsed with deionized water and then with isopropyl alcohol.

## 2.3. Measurement

Measurements were performed for both NiP coated guide samples. In addition, in order to measure the spin-flip probability of the copper guides (so we can subtract it from the measured spin-flip probability of the system that is composed of copper and NiP guides), measurements were made with the NiP samples removed. A description of the three configurations for which measurements were made is listed in Table 1. For all configurations, a series of measurements in which  $T_L$  was fixed and  $T_C$  was varied (loading time scan) and a series of measurements in which  $T_C$  was fixed and  $T_L$  was varied (cleaning time scan) were performed. Table 2 lists the values of  $T_C$  and  $T_L$  used for both the loading time and cleaning time scans.

An example of the neutron count rate as a function of time is shown in Fig. 2.

## 3. Data Analysis

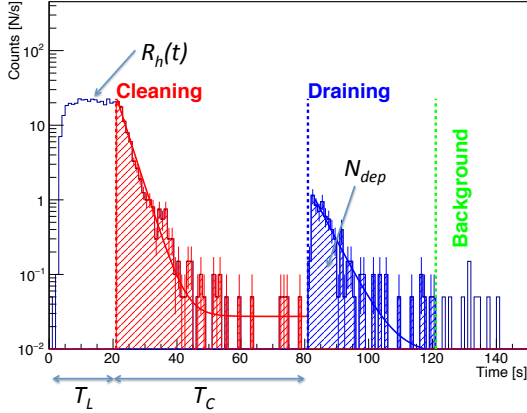
As mentioned earlier, Eq. (4) would allow determination of  $\beta$  from experimentally measured  $R_h(t)$

Table 1: Description of the three configurations for which measurements were performed

Configuration	Description	Cu guide length	NiP guide length
C1	SS guide with 50 $\mu\text{m}$ NiP coating	188 cm	100 cm
C2	Al guide with 50 $\mu\text{m}$ coating NiP	188 cm	100 cm
C3	No NiP coated guide	188 cm	0 cm

 Table 2: The values of  $T_C$  and  $T_L$  used for both the loading time scan and the cleaning time scan

Scan	$T_L$ (s)	$T_C$ (s)	Notes
Loading time scan	20, 40, 60, 80	20	
Cleaning time scan	60	10, 20, 40, 60, 80	$T_C = 80$ s is for C1 only.


 Figure 2: Neutron count rate as a function of time obtained for configuration C2 for  $T_L = 20$  s and  $T_C = 60$  s.

and  $N_{dep}$  if  $P(v, t)$  and  $\tau_{dep}(v)$  were known with sufficient accuracy.  $P(v, t)$  depends not only on the velocity distribution of the UCN entering the system but also on the lifetime of high-field seekers in the system  $\tau_{hfs}(v)$ , which we expect to be very close to the lifetime of low-field seekers,  $\tau_{dep}(v)$ .  $\tau_{hfs}(v)$  depends not only on the surface-UCN interactions but also on how the system was assembled, as for many systems the UCN loss can be dominated by gaps at joints between UCN guide sections.

In the absence of sufficiently accurate experimentally obtained information on  $P(v, t)$  and  $\tau_{dep}$ , we had to resort to analysis models in which approximations were made to Eq. (4) and evaluated the effect of those approximations to the extracted values of  $\beta$ . Below we describe the two specific analysis models we employed and the results obtained from these models.

### 3.1. Analysis model 1

In this model,  $\tau_{dep}$  is assumed to be independent of neutron velocity  $v$ . With this assumption, Eq. (4) simplifies to

$$N_{dep} = \beta \frac{A_{tot}}{A_h} \int_0^{T_L+T_C} R_h(t) e^{-\frac{T_L+T_C-t}{\tau_{dep}}} dt. \quad (5)$$

From the experimentally measured  $R_h(t)$  and  $N_{dep}$ , we obtained the values of  $\beta$  for a set of assumed values for  $\tau_{dep}$ . For the correct value of  $\tau_{dep}$ , the value of  $\beta$  should be independent of the values of  $T_L$  and  $T_C$ . Figure 3 shows plots of  $\beta$  for a set

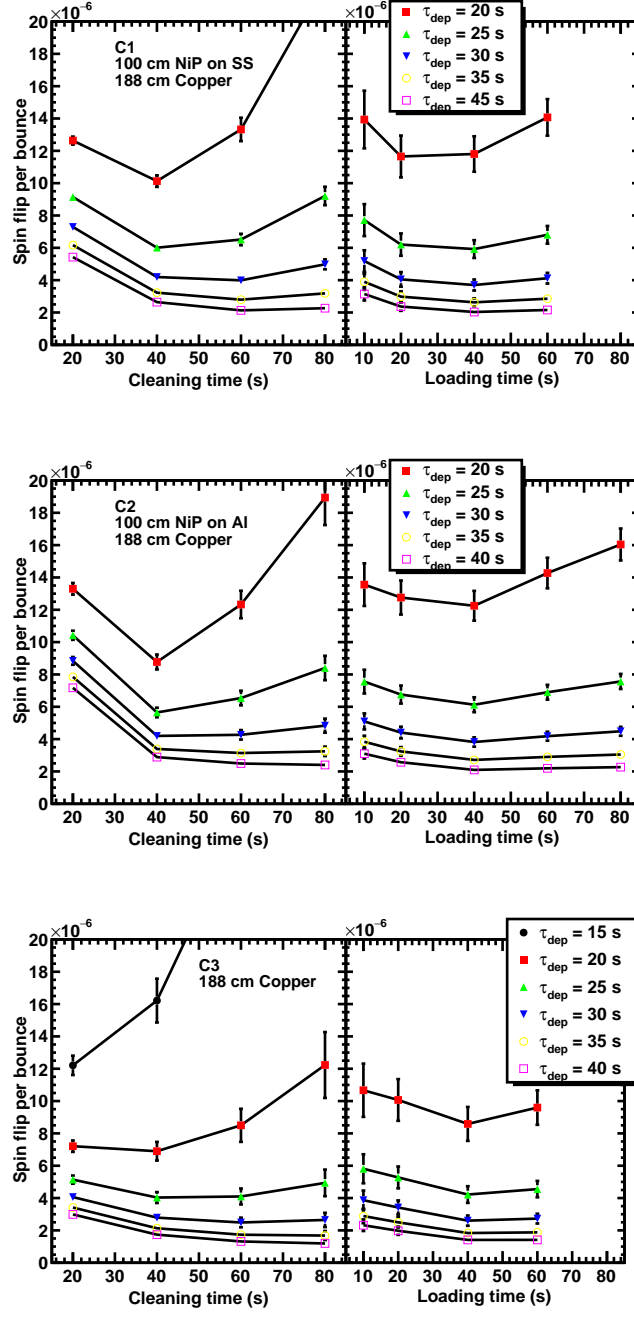


Figure 3: Plots of  $\beta$  for a set of values of  $\tau_{dep}$  for both the  $T_L$  and  $T_C$  scans obtained assuming Eq. (5)

of values of  $\tau_{dep}$  for both the  $T_L$  and  $T_C$  scans. For this analysis,  $N_{dep}$  was determined by integrating the counts over a counting period of 40 s after  $t = T_L + T_C$  and subtracting the background estimated from the counts after the counting period.

From these results we see the following:

- $\beta \sim 4 \times 10^{-6}$  can describe data for all combinations of  $T_L$  and  $T_C$  for all three configurations reasonably well except for  $T_C = 20$  s.
- The deviation for  $T_C = 20$  s is larger for configurations C1 and C2 than for configuration C3.

The deviation of the data points for  $T_C = 20$  s from other data points can be attributed to the fact that 20 s was not sufficiently long to remove all the high-field seekers and as a result there were high-field seekers included in what was counted as  $N_{dep}$ . From the simple kinetic theory formula  $\tau_{emp} = (4V)/(vA)$ , where  $\tau_{emp}$  is the emptying time,  $V$  is the volume of the container,  $A$  is the area of the hole,  $v$  is the velocity of the particle, the time it takes for the high seekers to be emptied can be estimated to be 4.25 s for configurations C1 and C2 (the total guide length = 425 cm) and 3.25 s for configuration C3 (the total guide length = 325 cm), assuming  $v = 400$  cm/s.

The “best fit” values of  $\beta$  and  $\tau_{dep}$  can be obtained by minimizing  $\chi^2$  defined as

$$\chi^2 = \sum_{i=\{T_C, T_L\}} \frac{\{\beta_i(\tau_{dep}) - \beta\}^2}{(\delta\beta_i)^2}, \quad (6)$$

where the summation is over all combinations of  $\{T_C, T_L\}$  except for  $T_C = 20$  s. The obtained best fit values of  $\beta$  and  $\tau_{dep}$  as well as the  $1\sigma$  boundary are graphically indicated in Fig. 4 for each configuration. The numerical results are listed in Table 3.

### 3.2. Analysis model 2

In this model, we assumed  $P(v) \propto v^2$ . The  $v^2$  dependence is well motivated from Monte Carlo simulations performed on the UCN production and transport [26]. Furthermore, for the UCN loss we assumed

$$\tau_{dep}(v) = \left( \frac{v}{4} \frac{A_{tot}}{V} f \right)^{-1}, \quad (7)$$

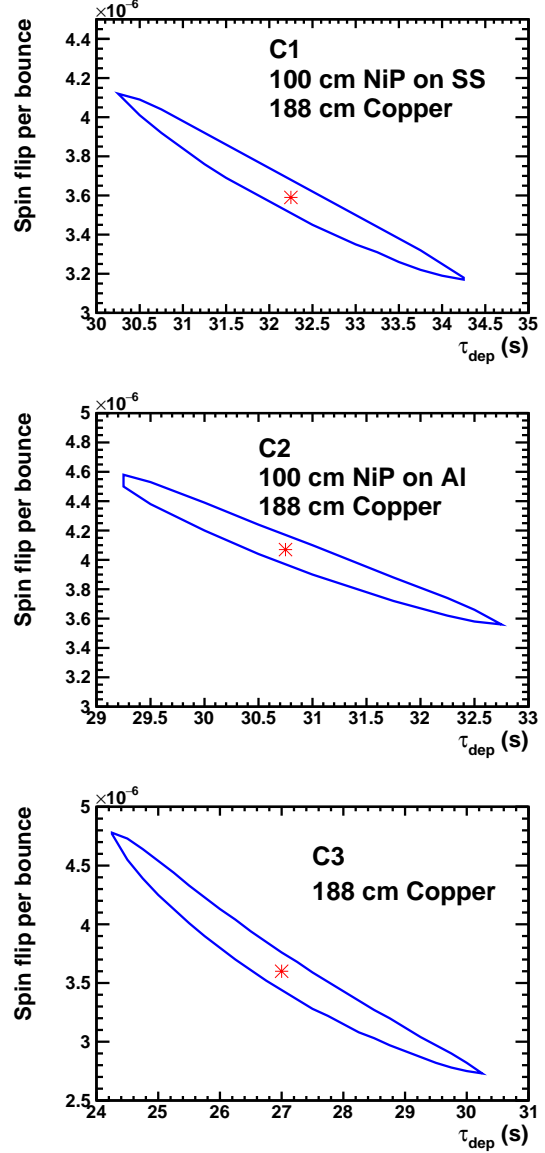


Figure 4: best fit values of  $\beta$  and  $\tau_{dep}$  as well as the  $1\sigma$  boundary for each configuration for analysis model 1.

Table 3: Results obtained from Analysis Model 1. Only the best fit values are listed for  $\tau_{dep}$ . For description of the guide configurations, see Table 1.

Guide	$\beta$	$\tau_{dep}$ (s)	$\chi^2/\text{DOF}$
C1	$(3.6^{+0.5}_{-0.4}) \times 10^{-6}$	32.3	1.49
C2	$(4.1^{+0.5}_{-0.5}) \times 10^{-6}$	30.3	0.94
C3	$(3.6^{+1.2}_{-0.9}) \times 10^{-6}$	27.0	0.84

where  $V$  is the volume of the trap and  $f$  is a factor corresponding to the probability of UCN loss per collision. In this model we assumed  $f$  to be independent of the UCN energy and the angle of incidence. This is a good approximation when UCN loss is dominated by gaps in the system, and not by the interaction of UCNs with walls, as it is the case for this system as shown below.

Substituting Eq. (7) into Eq. (4) with  $P(v) = \frac{3}{v_c^3} v^2$  and integrating over  $v$  yields

$$N_{dep} = \beta \frac{A_{tot}}{A_h} \frac{3}{v_c^3} \int_0^{T_L+T_C} dt R_h(t) \times \frac{2 + e^{-av_c} \{-2 - av_c(2 + av_c)\}}{a^3}, \quad (8)$$

where  $a = \frac{1}{4} \frac{A_{tot}}{V} f(T_L + T_C - t)$ .

From the experimentally measured  $R_h(t)$  and  $N_{dep}$ , we obtained the values  $\beta$  for a set of assumed values of  $f$  using Eq. (8) with  $v_c = 5.66$  m/s corresponding to the cutoff energy for copper. The “best fit” values of  $\beta$  and  $\tau_{dep}$  can be obtained by minimizing  $\chi^2$  defined as

$$\chi^2 = \sum_{i=\{T_C, T_L\}} \frac{\{\beta_i(f) - \beta\}^2}{(\delta\beta_i)^2}, \quad (9)$$

where the summation is over all combinations of  $\{T_C, T_L\}$  except for  $T_C = 20$  s. The obtained best fit values of  $\beta$  and  $f$  as well as the  $1\sigma$  boundary are graphically indicated in Fig. 5 for each configuration. The numerical results are listed in Table 4.

### 3.3. Discussion of the analysis results

While the two analysis methods yielded somewhat different values for  $\beta$ , in each analysis, the difference

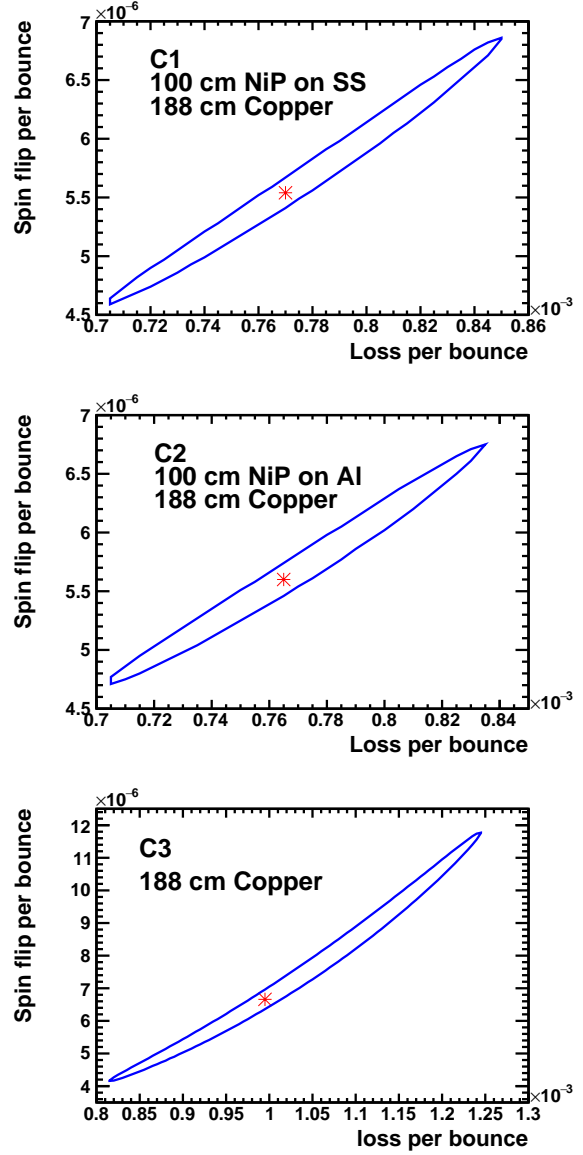


Figure 5: best fit values of  $\beta$  and  $\tau_{dep}$  as well as the  $1\sigma$  boundary for each configuration for analysis model 2.



Table 4: Results obtained from Analysis Model 2. Only the best fit values are listed for  $f$ . For description of the guide configurations, see Table 1.

Guide	$\beta$	$f$	$\chi^2/\text{DOF}$
C1	$(5.5^{+1.3}_{-1.0}) \times 10^{-6}$	$7.7 \times 10^{-4}$	0.99
C2	$(5.6^{+1.2}_{-0.9}) \times 10^{-6}$	$7.7 \times 10^{-4}$	0.97
C3	$(6.7^{+5.0}_{-2.5}) \times 10^{-6}$	$1.0 \times 10^{-3}$	0.99

in  $\beta$  among different guide configurations were small, indicating that the NiP coated guide sections were as non-depolarizing as copper guides.

Now we discuss possible systematic biases introduced in the results due to the simplifying assumptions made for each of the analysis models. In Analysis Model 1, it was assumed that the lifetime of the depolarized neutrons were the same regardless of the UCN velocity. It is usually the case that slower neutrons have a longer lifetime, because the loss rate is proportional to the rate of collision with the walls and also the loss per bounce for wall collision is larger for faster neutrons. This effect causes the average velocity of UCNs trapped for an extended period of time to be lower than the initial velocity. The assumption of velocity independent UCN lifetime ignores the possible spectral difference between the high-field seekers that initially occupied the system and the detected spin-flipped UCNs. Since the detected spin-flipped UCNs tended to have lower velocities than the initial high-field seekers, the estimation of the collision rate using the measured  $R_h$  is an overestimate for the detected spin-flipped UCNs. This resulted in an underestimate of the spin flip probability  $\beta$ .

Analysis Model 2 cures this problem. It describes UCN loss with a single parameter, the loss per bounce  $f$ , which is independent of the UCN velocity. As mentioned earlier, this is a good approximation when the UCN loss is dominated by gaps in the system. In fact, the obtained values of  $f$  are  $\sim 10^{-3}$ , much larger than the typical loss per bounce for loss due to collision with walls.  $f \sim 10^{-3}$  indicates that there was a 1 mm wide gap every 1 m of guide, which is reasonable considering how the system was put together. Note that the effect of the pin hole is much smaller. The contribution from the pinhole to  $f$  is  $\sim 2.8 \times 10^{-5}$  for

C1 and C2 and  $f \sim 1.3 \times 10^{-5}$  for C3.

The values of  $\beta$  obtained from Analysis Model 2 are larger than those from Analysis 1 by a factor of 1.4-1.9. This can be explained by the underestimation on the values of  $\beta$  for Analysis Model 1 that was discussed earlier. The size of this effect can be estimated as follows. For a neutron velocity spectrum proportional to  $v^2$ , the average velocity is  $v_{ave} = \frac{3}{4}v_c$ . If the UCN loss is described by a constant loss per bounce  $f$ , then the average velocity of the UCN after time  $t$  is

$$\begin{aligned}
 v_{ave}(t) &= \frac{\int_0^{v_c} v^3 e^{-bvt} dv}{\int_0^{v_c} v^2 e^{-bvt} dv} \\
 &= \frac{6 + e^{-c}[-6 - c\{6 + c(3 + c)\}]}{bt[2 + e^{-c}\{-2 - c(2 + c)\}]}, \quad (10)
 \end{aligned}$$

where  $b = \frac{1}{4} \frac{A_{tot}}{V} f$  and  $c = b t v_c$ . Inserting the values from this experiment of  $v_c = 5.66$  m/s,  $4V/A_{tot} = 7.62$  cm, and  $f = 0.7 \times 10^{-3}$  gives  $\frac{v_{ave}(t)}{v_{ave}(0)} \simeq 1.5$  for *e.g.*  $t = 100$  s, consistent with the observation made with the comparison between Analysis Models 1 and 2.

Both analysis results indicate that the UCN loss was smaller when a NiP coated guide section was included in the system than it was when the system was solely made of copper guides. This can be attributed to two factors: (1) the smaller average number of gaps per unit length when the NiP coated guide is included in the system as the NiP coated section is longer than the other guide section (see Fig. 1), and (2) the superior UCN storage properties of NiP coated guides that we observed [22], which in turn is due to the higher Fermi potential of NiP.

Assuming that UCN were uniformly distributed inside the system we can relate the UCN spin flip probabilities obtained for configurations C1 and C2 to the UCN spin flip probability for NiP coated surfaces and that for copper surfaces determined by configuration C3. That is

$$\beta_{C1,C2} = f_{Cu} \beta_{Cu} + f_{NiP} \beta_{NiP}, \quad (11)$$

where  $f_{Cu}$  and  $f_{NiP}$  are the fraction of the copper surface and that of the NiP coated surface in the system. Note  $f_{NiP} = 0.35$ ,  $f_{Cu} = 0.65$ , and  $\beta_{Cu} =$

Table 5: Values of the spin-flip probability per bounce  $\beta$  determined from our work

Material	$\beta$
NiP on 316L SS	$(3.3^{+1.8}_{-5.6}) \times 10^{-6}$
NiP on Al	$(3.6^{+2.1}_{-5.9}) \times 10^{-6}$
Copper	$(6.7^{+5.0}_{-2.5}) \times 10^{-6}$

$\beta_{C3}$ . The results obtained from Eq. (11) and the results of Analysis Model 2 listed in Table 4 are shown in Table 5. Here we assumed that the uncertainties on  $\beta_{C1}$ ,  $\beta_{C2}$ , and  $\beta_{C3}$ , which are dominated by the uncertainties on the loss per bounce parameters, are 100% correlated.

The uncertainties of our results were dominated by the uncertainty on the value of the loss per bounce for UCN stored in the system. The uncertainty can be significantly reduced by making an auxiliary measurement to determine this parameter, if a similar experiment is to be performed in the future experiment. This could be achieved by, for example, performing a measurement without opening the shutter and observing the rate at which the depolarized neutrons leak through the pinhole on the shutter, if there was a sufficiently high UCN density stored in the system. Also studying the energy dependence of the depolarization probability is of great interest, as it may shed light on the mechanism of UCN depolarization. Such a study can be performed by repeating measurements described in this paper for different magnetic field values for the superconducting magnet thus varying the cutoff energy of the stored neutrons, as was done in Ref. [11]. Such a study of energy dependence would also allow a determination of the energy dependence of the UCN loss parameter.

#### 4. Discussion

Our results indicate that the depolarization per bounce on the surface of NiP coated 316L SS as well as NiP coated Al is as small as that of copper surfaces. 316L stainless steel is austenitic and is considered to be “non-magnetic.” However, stress, due to cold working, can cause it to develop martensitic microstructure. Such surface magnetism is likely to

be the reason for the large depolarization probability observed previously. The 50  $\mu\text{m}$  thick NiP coating seems to be sufficiently thick to keep UCN from “seeing” the magnetic surface.

As mentioned earlier, NiP coating is extremely robust and is widely used in industrial applications. The coating can be applied commercially in a rather straightforward chemical process and there are numerous vendors that can provide such a service rather inexpensively. The ability of NiP coatings to turn SS surfaces non-depolarizing has many practical implications. SS UCN guides are widely used in UCN facilities because of its mechanical robustness and its relatively high UCN potential. However, because of its highly depolarizing nature, other guide materials, such as quartz guides coated with DLC or nickel molybdenum, have so far been used when non-depolarizing guides were needed. Simple NiP coatings can turn SS surfaces non-depolarizing. In addition, NiP has a higher Fermi potential than SS. We have confirmed that SS flanges retain their sealing properties even after they are coated with NiP. Therefore NiP coated SS guides can be used where both mechanical robustness as well as non-depolarizing properties are required. One such application is cryogenic UCN sources, such as the one being constructed at TRIUMF [27].

#### 5. Summary

We measured the spin-flip probabilities for ultracold neutrons interacting with surfaces coated with nickel phosphorus. For 50  $\mu\text{m}$  thick nickel phosphorus coated on stainless steel, the spin-flip probability per bounce was found to be  $\beta_{\text{NiP on SS}} = (3.3^{+1.8}_{-5.6}) \times 10^{-6}$ . For 50  $\mu\text{m}$  thick nickel phosphorus coated on aluminum, the spin-flip probability per bounce was found to be  $\beta_{\text{NiP on Al}} = (3.6^{+2.1}_{-5.9}) \times 10^{-6}$ . For the copper guide used as reference, the spin flip probability per bounce was found to be  $\beta_{\text{Cu}} = (6.7^{+5.0}_{-2.5}) \times 10^{-6}$ .

Our results indicate that NiP coatings can make SS surface non-depolarizing. In addition, NiP has a higher Fermi potential than SS. This will open wide possibilities in UCN guide technology.

## Acknowledgments

This work was supported by Los Alamos National Laboratory LDRD Program (Project No. 20140015DR). We gratefully acknowledge the support provided by the LANL Physics and AOT Divisions.

## References

## References

- [1] D. Dubbers and M. G. Schmidt, Rev. Mod. Phys. **83**, 1111 (2011).
- [2] A. R. Young, *et al.* J. Phys. G: Nucl. Part. Phys. **41**, 114007 (2014).
- [3] A. Steyerl, *et al.*, Phys. Lett. A **116**, 347 (1986)
- [4] A. Saunders, *et al.*, Rev. Sci. Instrum. **84**, 013304 (2013).
- [5] Y. Masuda, *et al.*, Phys. Rev. Lett. **108**, 134801 (2012)
- [6] H. Becker, *et al.* Nucl. Instrum. Methods Phys. Res. A **777**, 20 (2015).
- [7] Th. Lauer and Th. Zechlau, Eur. Phys. J. A **49**, 104 (2013).
- [8] A. Serebrov, *et al.*, Nucl. Instrum. Methods Phys. Res. A **440**, 717 (2000).
- [9] Yu. N. Pokotilovski, JETP Lett. **76**, 162 (2002).
- [10] A. P. Serebrov, *et al.* Phys. Lett. A **313**, 373 (2003).
- [11] F. Atchison, *et al.* Phys. Rev. C **76**, 044001 (2007).
- [12] D. J. Salvat, *et al.*, Phys. Rev. C **89**, 052501(R) (2014).
- [13] C. A. Baker, *et al.*, Phys. Rev. Lett **97**, 131801 (2006).
- [14] B. Plaster, *et al.*, Phys. Rev. C **86**, 055501 (2012).
- [15] M. Mendenhall, *et al.*, Phys. Rev. C **87**, 032501(R) (2013).
- [16] M. Makela, PhD Thesis, Virginia Polytechnic Institute and State University, 2005.
- [17] R. Rios, APS Meeting Abstract BAPS.2009.APS.C14.3 (2009).
- [18] A. T. Holley, PhD Thesis, North Carolina State University (2012).
- [19] V. V. Vladimirkii, Sov. Phys. JETP **12**, 740 (1961).
- [20] R. L. Gamblin and T. R. Carver, Phys. Rev. **138** A946 (1965).
- [21] Y. Masuda (private communication).
- [22] R. W. Pattie Jr., *et al.*, in preparation.
- [23] Los Alamos National Laboratory LDRD Project #20140015DR, “Probing New Sources of Time-Reversal Violation with Neutron EDM”, Takeyasu Ito, PI.
- [24] T. M. Ito, *et al.*, in preparation.
- [25] Valex Corp. <http://www.valex.com>.
- [26] S. M. Clayton (unpublished).
- [27] J. W. Martin *et al.*, AIP Conf. Prof. **1560**, 134 (2013).